Poussou, S.B., Mazumdar, S., Plesniak, M.W., Sojka, P.E., and Chen, Q. 2010. "Flow and contaminant transport in an airliner cabin induced by a moving body: model experiments and CFD prediction," *Atmospheric Environment,* 44(24), 2830-2839.

Flow and contaminant transport in an airliner cabin induced by a moving body: Model experiments and CFD predictions

Stephane B. Poussou[1] **Sagnik Mazumdar**[1]
Michael W. Plesniak[1,2] **Paul E. Sojka**[1] **Qingyan Chen**[1,*]

[1]National Air Transportation Center of Excellence for Research in the Intermodal Transport Environment (RITE)
School of Mechanical Engineering, Purdue University, West Lafayette, IN 47907

[2]Department of Mechanical and Aerospace Engineering
The George Washington University, Academic Center, Washington DC 20052

Abstract: The effects of a moving human body on flow and contaminant transport inside an aircraft cabin were investigated. Experiments were performed in a one-tenth scale, water-based model. The flow field and contaminant transport were measured using the Particle Image Velocimetry (PIV) and Planar Laser-Induced Fluorescence (PLIF) techniques, respectively. Measurements were obtained with (ventilation case) and without (baseline case) the cabin environmental control system (ECS). The PIV measurements show strong intermittency in the instantaneous near-wake flow. A symmetric downwash flow was observed along the vertical centerline of the moving body in the baseline case. The evolution of this flow pattern is profoundly perturbed by the flow from the ECS. Furthermore, a contaminant originating from the moving body is observed to convect to higher vertical locations in the presence of ventilation. These experimental data were used to validate a Computational Fluid Dynamic (CFD) model. The CFD model can effectively capture the characteristic flow features and contaminant transport observed in the small-scale model.

Keywords: PIV, PLIF, CFD, Contaminant Transport, Aircraft Cabin, Ventilation, Human Wake

INTRODUCTION

In-flight transmission can potentially lead to a global dissemination of infectious disease agents, as two billion people travel every year (Joseph at al., 2003; Gendreau and DeJohn, 2002). Airborne infectious diseases transmitted in airliners include tuberculosis, influenza, measles, mumps, and SARS (Musher, 2003; CDC 2006). In a SARS-infected Air China Flight 112 from Hong Kong to Beijing on March 15, 2003, five passengers died after likely transmission from an infected passenger on the same flight (Olsen et al., 2003; Lakshmanan, 2003). Previous investigations have suggested that in-flight transmission of a disease contaminant should be confined within two rows of a contagious passenger (NRC 2002; Jeffrey et al., 1993; Kenyon et al., 1996). However, it has been observed that passengers

*Corresponding author. Tel.: +765-496-7562, Email address: yanchen@purdue.edu

seated as far as seven rows from the infected passenger can be contaminated (Olsen et al., 2003). Contaminant transmission and personal exposures have been shown to be significantly influenced by movement of individuals inside enclosed environments similar to airliner cabins (Brohus et al., 2006; Bjørn and Nielsen, 2002; Bjørn et al., 1997). Moreover, in some in-flight transmission incidents like the Air China flight, crew members were infected, which raises concerns about the mechanisms of transmission, i.e. whether their movement aided contamination. In that context, the present investigation is an attempt to understand the influence of moving crew members and passengers on flow and contaminant transport in an airliner cabin.

The study of the influence of human movements on airborne contaminant transmission in airliner cabins can be done experimentally or through computer simulations. Carefully-designed laboratory experiments with controlled thermo-fluid conditions provide accurate and useful information. However, the airliner cabin configuration and thermo-fluid conditions can vary considerably, making experimental investigations under varied cabin circumstances time-consuming, expensive and difficult (Mazumdar and Chen, 2008). Therefore, measured data from a properly controlled laboratory experiment are usually used to test the performance of versatile and efficient numerical models, which may be used to further study the influence of variations in cabin configuration and thermo-fluid conditions. Numerical simulations of movement in a cabin can be handled using direct or indirect numerical methods. Direct methods are more time-expensive because they involve moving and dynamic grids to simulate body movement. Matsumoto et al. (2004) and Shih et al. (2007) used dynamic grid deformation approaches to generate the computational mesh around the moving body in an empty room and an isolation room, respectively. Choi and Edwards (2008) modeled contaminant transport induced by a person walking from one room to another, and from a room into a long hallway.

On the other hand, indirect methods are used to model movements in an approximate way, as with a distributed momentum source (Zhai et al., 2002) or a turbulent kinetic energy source (Brohus et al., 2006). Indirect methods are computationally faster, since they require no remeshing, and are therefore preferred over direct methods. Moreover, any real-life body displacement pattern may be modeled using indirect methods, which might be beyond practical reach using direct methods, however at the expense of accuracy (Brohus et al., 2006). Both direct and indirect numerical simulation of persons' movement has its own pros and cons, yet the reliability of the CFD modeling techniques in predicting flow and contaminant transport in enclosed environments like airliner cabins is still inconclusive. Unless validated by high quality experimental data, the reliability of the approximations made in the CFD models would remain questionable (Chen and Srebric, 2002).

The literature on experimental investigations of diverse enclosed environments reports the significant influence of movement on airflow and transport of contaminants (Matsumoto and Ohba, 2004; Bjørn and Nielsen, 2002; Bjørn et al., 1997; Mattsson and Sandberg, 1996). However, these studies had insufficient spatial and temporal resolutions for validation of CFD models. Moreover, studies recently conducted by Zhang et al. (2005; 2009) and Kühn et al. (2009) emphasized the difficulty to measure and understand the complex airflow inside a full-scale cabin mockup, even under steady-state conditions. The large volume of the

enclosure and complications arising from obstructions such as seats and simulated passengers prevented obtaining detailed data. In addition, the presence of body movement would make it more difficult to acquire data with meaningful resolutions. On the other hand, small-scale water models produce reasonably well-resolved data to permit an understanding of flow and contaminant transport in ventilated buildings, e.g. Lin and Linden (2002), Thatcher et al. (2004), Settles (2006), and Finlayson et al. (2004). As a consequence, the present study uses a simplified small-scale cabin mockup inside a water tank in an effort to generate high-quality experimental data required to validate the performance of an associated CFD model. However, changes in the physical scale and working fluid further complicate interpretation of equivalent effects in the full-scale (Thatcher et al., 2004).

In order to address the influence of body movement on flow and contaminant transport in airliner cabins comprehensively, the results of the investigation would be presented in two paper series. This first paper presents the experimental results from the small-scale cabin mockup and discusses the performance of a companion CFD model.

EXPERIMENTAL METHODS

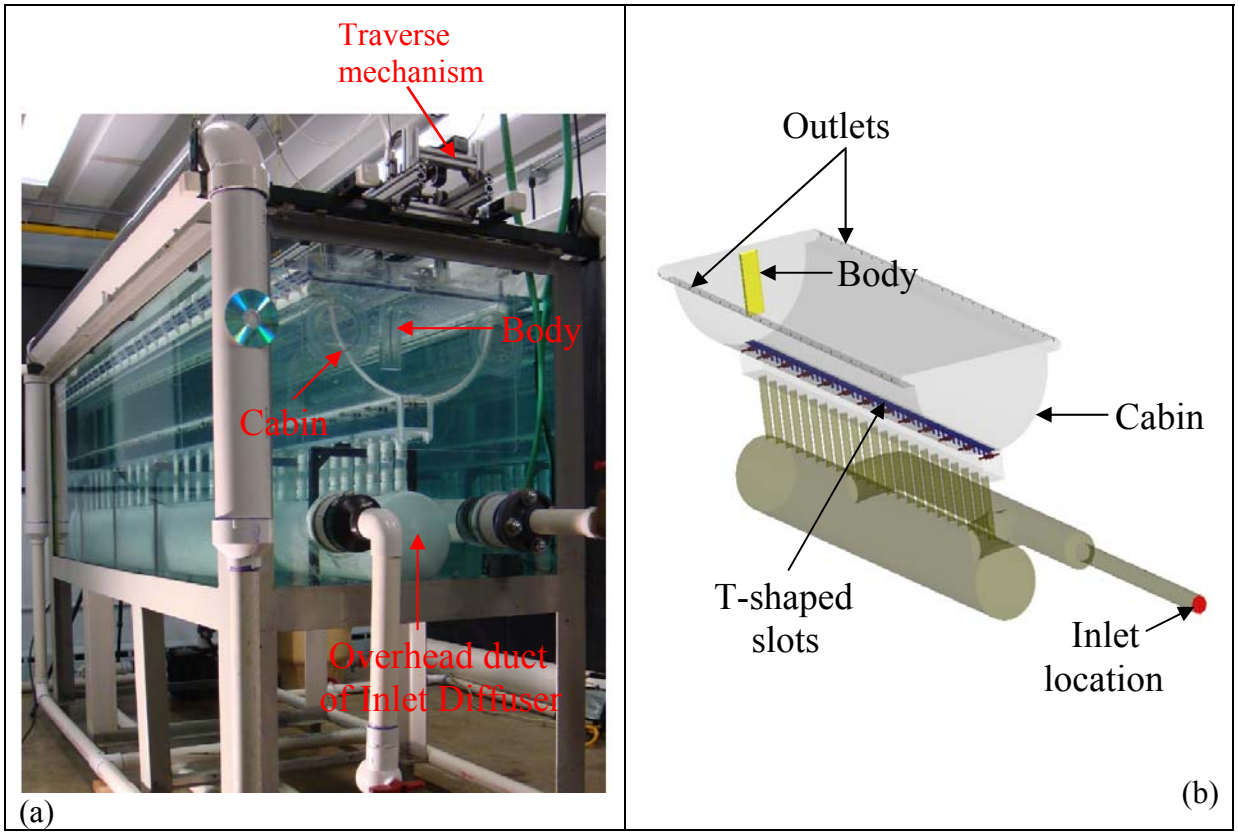

Figure 1. (a) The small-scale experimental test facility of the cabin mockup; and (b) the CFD model of the test facility

Experimental setup

Figure 1(a) shows the small-scale, water-based experimental test facility consisting of an upside-down cabin mockup. The cabin was made using a transparent, semi-circular pipe of 45 cm diameter and 2.44 m length. The one-tenth-scaled mockup, fully submerged in a glass tank, was equivalent to a cabin with 28 rows of economy-class seats. Water temperature was monitored during each experiment to maintain isothermal conditions inside the cabin so that buoyancy effects could be neglected. The interior of the modeled cabin was free of obstructions to eliminate secondary flow features. To simulate the environmental control system (ECS) of commercial airliner cabins, provisions were made to inject water through an overhead duct of the inlet diffuser assembly (Fig. 1(a)).). Water was pumped to the overhead pipe from a 550-liter tank. To achieve uniform inflow into the cabin, the water entered a settling chamber through 23 pipe fittings and was then supplied to the cabin through 48 elongated openings cut along the length, where a T-shaped diffuser diverted the fluid laterally to both sides of the cabin cross-section. Water was extracted from two outlets located near the side walls of the cabin at floor level. An automated mechanism placed above the experimental facility traversed the body (0.02 m thick x 0.05 m wide x 0.17 m tall) along the longitudinal direction of the cabin. A simplified body geometry was selected for modeling simplicity and to gain a better understanding of flow and contaminant transmission phenomena associated with a moving body. In order to isolate the effects of the moving body, measurements were done with (ventilation case) and without (baseline case) the environmental control system (ECS), respectively.

Experimental Techniques

Particle Image Velocimetry (PIV) was employed to measure the velocity distribution inside the water tank, using a dual 50 mJ/pulse NewWave Gemini Nd:YAG laser (Raffel et al., 2007). Table 1 presents the parameters of the PIV system. The time interval between two successive laser pulses was typically between 1500 and 2500 μs. A digital camera (2,048×2,048 pixels PowerView 4MP) was used to acquire images. The CCD camera and laser were positioned to capture cross-sectional and longitudinal flow images (Fig. 2). The flow visualization images were obtained using 14 μm diameter silver-coated, hollow-sphere particles with specific gravity of 1.7. A program was written (Labview) to synchronize the motion of the moving body with the data acquisition system. The body speed was 0.175 m/s at the model scale, which is equivalent to moving through two economy-class rows per second in an actual airliner cabin under kinematically similar conditions. Under Reynolds number equivalence of flow over the moving body in the water-based small-scale model and a full-scale airliner, this speed is equivalent to 0.25 m/s for a full-scale airliner with air as the working fluid. Settles (2006) indicated that the human aerodynamic wake replaces the thermal plume effects from the moving body if the speed exceeds 0.2 m/s. Thus the isothermal flow features observed in the baseline case can be used by future researchers for validation of full-scale cases with a moving body having the same Reynolds number. The time and velocity scales of the tracer particles for the small-scale cabin under the given conditions are shown in Table 2. Since the tracer particles have a particle Stokes number much less than unity, the particles are expected to follow the fluid faithfully (Samimy and Lele, 1991). The physical resolution of the flow field was 3.5×3.5 mm. The experimental

uncertainties on the body velocity, the flow rate and the fluid mean velocity were ± 0.4%, ± 4% and ± 5.2% respectively (Poussou, 2008).

Table 1. Parameters for the PIV system

Component	Description	Characteristics
Laser	New Wave, Gemini PIV Model #105355	Nd:YAG, 15 Hz, 532 nm 5 ns pulse, 50 mJ/pulse
Camera	TSI Inc., PowerView 4MP Model #630159	12-bit gray levels 2048x2048 pixels Nikon AF Micro-NIKKOR 60mm Nikon 62mm Circular Polarizer II
Computer	Dell T3400, Intel Dual Core	2.4 GHz, 2 Gb RAM
Software	TSI Inc., Insight 3G v8.0.5	
Optics	TSI Inc., cylindrical lenses TSI Inc., spherical lenses	-15, -25, -50 mm 250, 500, 1000 mm
Particles	Laboratory for Experimental Fluid Mechanics at the Johns Hopkins University	Silver coating 14 µm diameter Specific Gravity = 1.7

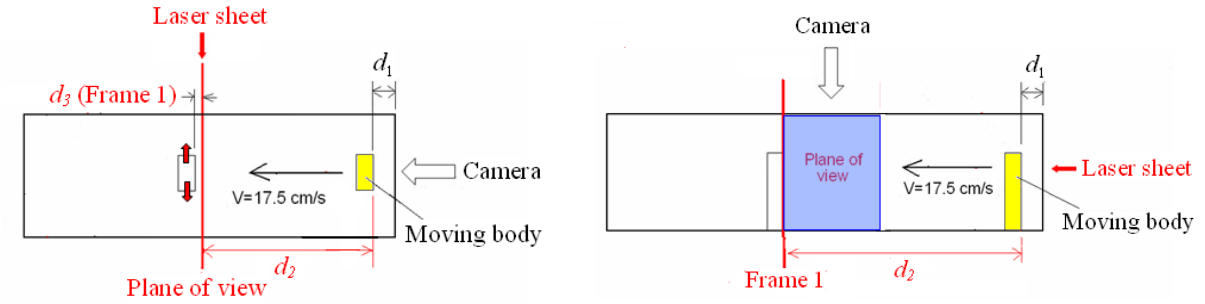

(a) (b)

Experimental settings		
	Baseline	With Ventilation
Flow rate (L/s)	0	2.5
Cross-sectional view	d_1 = 16.6 cm d_2 = 83.1 cm d_3 = 1.0 cm	d_1 = 9.4 cm d_2 = 34.2 cm d_3 = 1.0 cm
Longitudinal view	d_1 = 16.6 cm d_2 = 103 cm	d_1 = 9.4 cm d_2 = 63.8 cm

Figure 2. Schematic diagrams and experimental settings for (a) cross-sectional and (b) longitudinal flow visualizations.

Table 2. Tracer particle characteristics

Parameter	Value
Particle response time, τ_p	37.5 μs
Flow time scale, τ_f	3.6 ms
Gravitational settling time	3.2 μm/s
Centripetal settling time	723 μm/s
Particle Stokes number, $St = \tau_p/\tau_f$	0.0104

Table 3. Parameters for the PLIF system

Component	**Description**	**Characteristics**
Dye	ScholAR Chemistry, CAS #518-47-8	Disodium salt, $C_{20}H_{10}O_5.2Na$
Laser 1	New Wave, Gemini PIV, Model #10535	Nd:YAG, 532 nm
Laser 2	Lexel, Model #85	Ar-ion, 514.5 nm
Camera	TSI Inc., PowerView 4MP, Model #630159	12-bit gray levels, 7.25 fps 2048x2048 pixels

Planar Laser-Induced Fluorescence (PLIF) was used to visualize contaminant transport inside the small-scale airliner cabin (Freymuth, 1993). Contaminant was simulated by injecting a dye (uranine, $C_{20}H_{10}O_5.2Na$) into the flow and observing its fluorescence under laser illumination. In the present study, the dye was released from the lateral sides of the moving body (the red arrows Fig. 2 (a)). The details of the PLIF system are given in Table 3. The dye was delivered from an 18-liter container, pressurized to 48 kPa by compressed air, which emanated from the moving body at flow rates of 25 mL/s. Upon injection in the flow, the dye was illuminated by a 1-mm-thick laser sheet and recorded by a video camera as described in Table 3. Cylindrical optical lenses were used to form the laser sheet. Continuous movies of the flow were recorded and converted to frame sequences using standard video-editing methods (Adobe Premiere CS3). The frame sequences of the dye transport were used to qualitatively test the CFD model.

CFD MODELING

The CFD model used a second-order upwind scheme and the SIMPLE algorithm (Ferziger and Peric, 2002). The Re-Normalization Group (RNG) k-ε was used to model the turbulent flow. Compared to other turbulence models, RNG k-ε was observed to deliver the best performance in terms of accuracy, computing efficiency, and robustness for modeling indoor environments (Zhang et al., 2007). Note that the above CFD model would predict averaged flow field while the flow visualization images captured using PIV are instantaneous. Hence,

the average flow fields computed by CFD were compared with phase-averaged flow fields measured by PIV.

The CFD geometry used for this study is shown in Figure 1(b). Most of the geometrical features of the experimental test facility were accurately modeled, including the pipelines of the simulated environmental control system that supply water to the cabin through the inlet diffusers. The CFD model used a combined dynamic and static mesh scheme. The computational domain was divided into two separate sections: section 1 for the moving body (dynamic mesh, 0.25 million cells) and section 2 for the rest of the cabin (static mesh, 4.4 million cells), as illustrated in Figure 3. Only 5.3 % of the total meshes inside the domain were dynamic, thus reducing computing time required for remeshing. The maximum mesh size inside the cabin was 5 mm. The dynamic layering meshing scheme was used to keep the grid size in the dynamic zone constant which reduced the uncertainties due to size variation of the computational mesh (Brohus et al., 2006). A commercial CFD program, FLUENT (2003), was used for this study. The interactions between the static and dynamic sections were done using interfacing which can reduce the accuracy of the flow predictions (Tezduyar, 2004). User-defined functions were implemented in FLUENT to define and track the movement of the body.

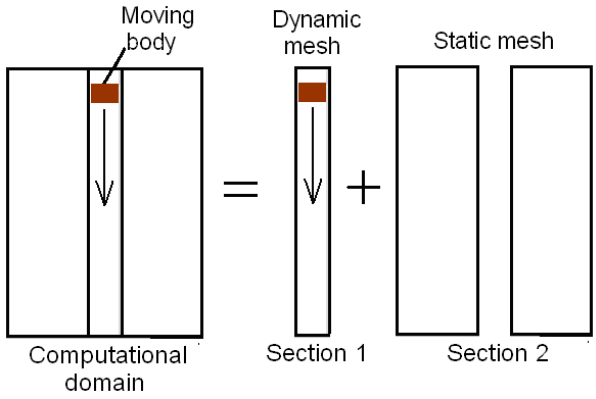

Figure 3. Layout of meshing scheme in the cabin section

Both cases, i.e. with and without ventilation, were computed in a 4-node Linux cluster. Each node had five processors (1.8 GHz AMD 64) and 4GB of memory. The time step used for the computations was 0.01 s.

RESULTS AND DISCUSSION

1. Cross-sectional Flow

1.1. Baseline case

Figure 4 shows instantaneous velocity fields in a cross-section at Frame 4 obtained during different runs (runs 1, 50, and 100, respectively) at different instants, along with the averaged velocity field obtained over one hundred runs. The speed of the body in the water was 0.175

m/s. Frame 4 was acquired when the back of the body is at a distance of 8.25 cm from the fixed laser sheet (see Figure 2). Figure 4 shows strong intermittency in the flow. Vertical symmetry in the wake was observed in the mean velocity field. Stochastic convergence using 25, 50 and 100 measurements is shown in Fig. 5. Vertical symmetry in the wake becomes visible after phase-averaging twenty five measurements.

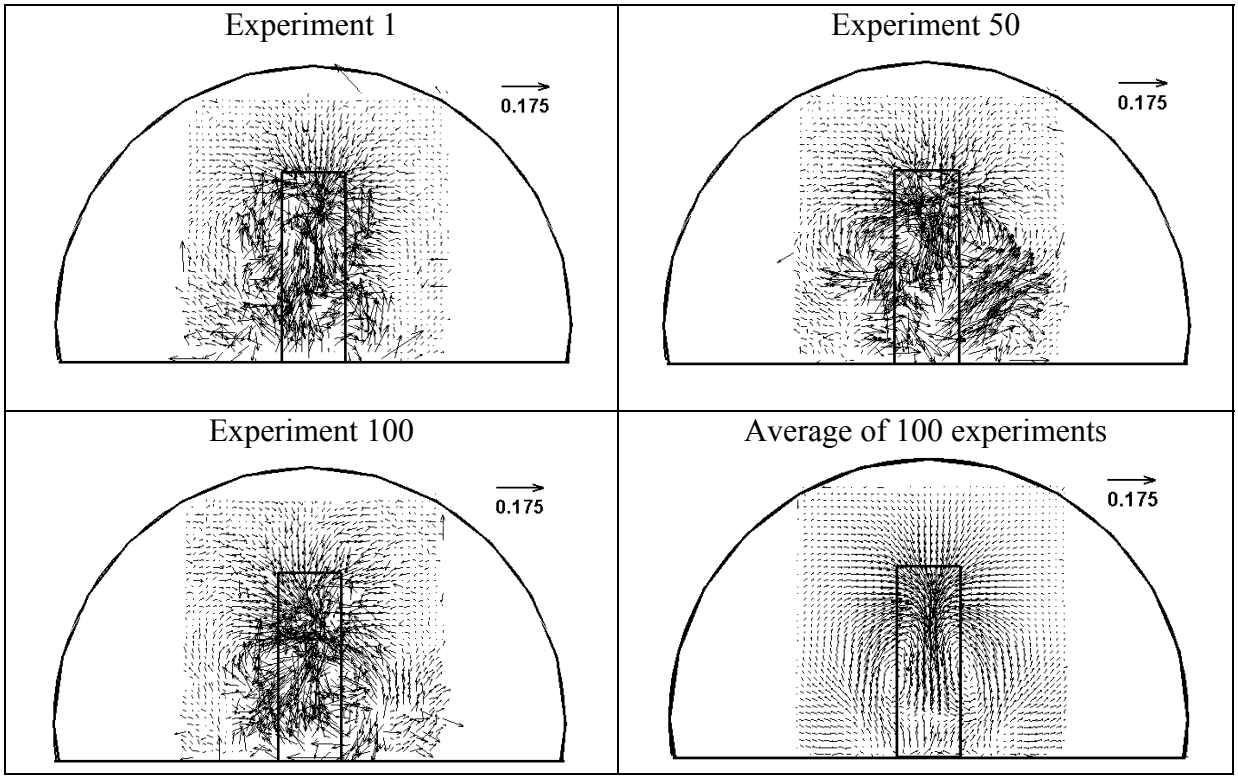

Figure 4. Instantaneous and averaged velocity fields at Frame 4 for the baseline case

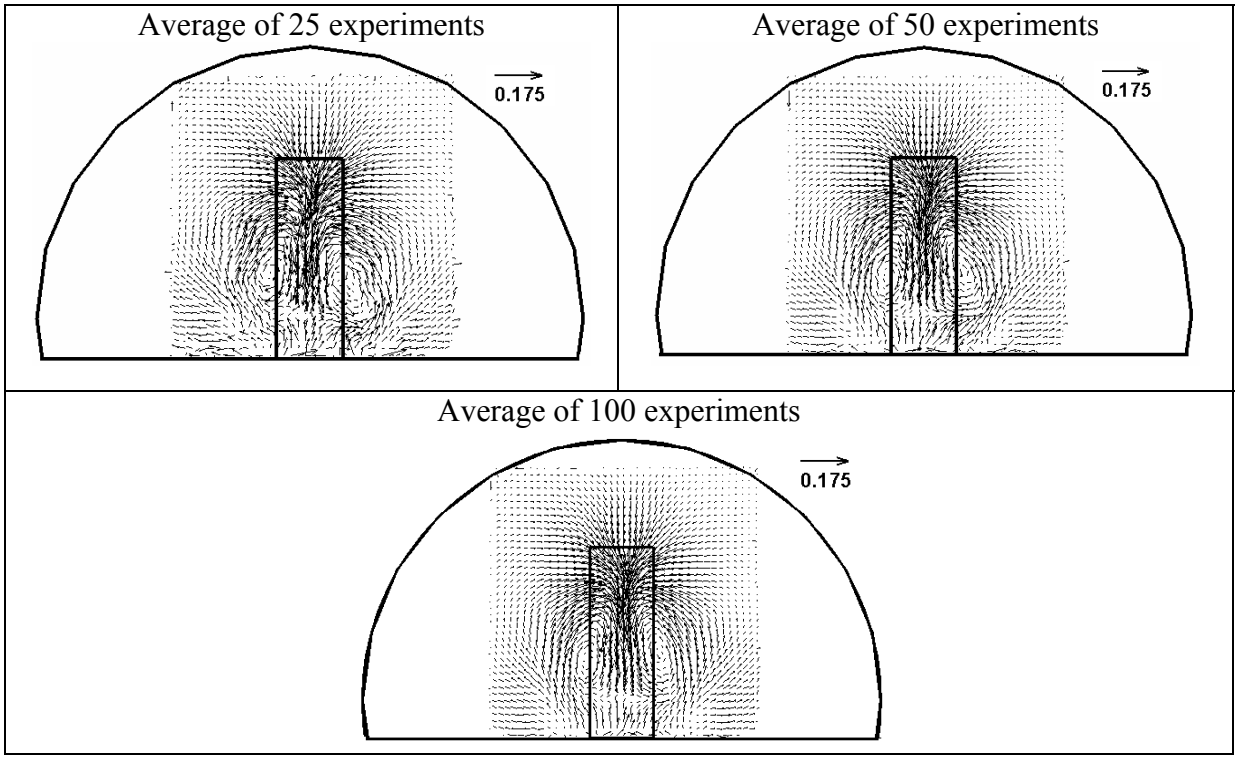

Figure 5. The averaged velocity fields at Frame 4 for the baseline case

Figure 6(a) shows the mean flow fields of one hundred measurements for baseline flow at Frames 1, 4 and 7, which were acquired when the back of the body moved 1, 8.25 and 15.5 cm past the laser sheet (refer to Figure 2), respectively. A strong downwash in the wake of the moving body is observed in Fig. 6, which is produced by the two symmetric eddies around the top corners. As the two eddies approached the cabin floor, they spread to the sides and were dissipated. The disturbance created by the moving body on the stagnant flow field diminished very rapidly after this process.

Figure 6(b) shows the corresponding computed flow field for Frames 1, 4 and 7 respectively. Side-by-side comparison indicates that the CFD model is able to predict the development of the two-eddy system. Though the predicted core size, flow pattern and structure agree, noticeable differences exist with respect to vortex aspect ratio. Reduction of mesh size and shifting of the interface boundary between the static and dynamic mesh zones did not alter the CFD predictions. Separated flows behind bluff bodies are typically difficult to model, e.g. transient RANS simulations by Lubcke (2001). However, the agreement of results with experimental data suggests that the CFD model can reasonably describe the flow physics of the baseline case which is a preliminary step to study contaminant transport in airliner cabins.

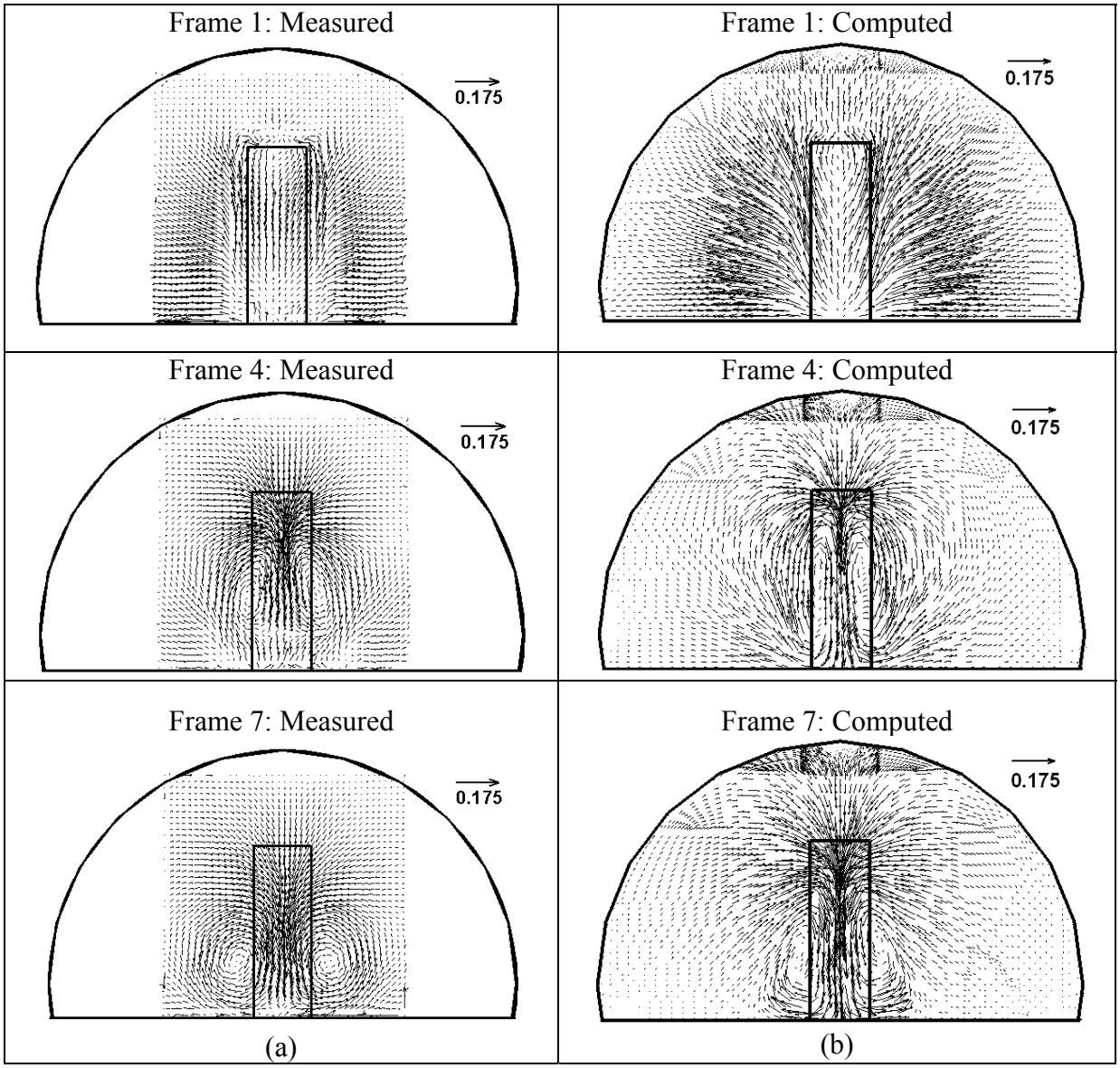

Figure 6. The (a) measured and (b) computed mean flow fields at Frames 1, 4 and 7 for the baseline case

1.2. Ventilation case

The cross-sectional flow of the ventilated cabin, when the ECS is operating, is shown in Fig. 7 at different instants. As in the baseline case, Fig. 7 shows the mean flow fields at t=0s and at Frames 4 and 7. The flow field at t=0s corresponds to the undisturbed flow generated by the ECS, before the body started its movement. The injection of water coming into the cabin through the overhead duct of the inlet diffuser assembly (refer to Fig. 1(a)) is evident from the CFD results in Fig. 7(b). The PIV measurements in Fig. 7(a) do not show these incoming

jets as the measurement window was focused inside the cabin. The CFD model captured the steady-state vortices across the cross-section much more accurately than in previous attempts (Zhang et al., 2009). This is due to accurate modeling of inlet geometrical features of the experimental setup. The average cross-sectional airflow (at t=0 s) shows a quasi-symmetric vortex structure. The assembly of the experimental setup did not permit perfect symmetry in the flow. The particular section shown in Figure 7 showed the best flow symmetry. Flow asymmetry has also been observed in aircraft cabins due to an inherent instability in the combined vortex structure across the cabin cross-section (Lin et al., 2005). An asymmetry is likely to be present even if the apparatus was perfectly symmetric. It is thus noteworthy that the CFD model captured this asymmetric flow pattern reasonably well.

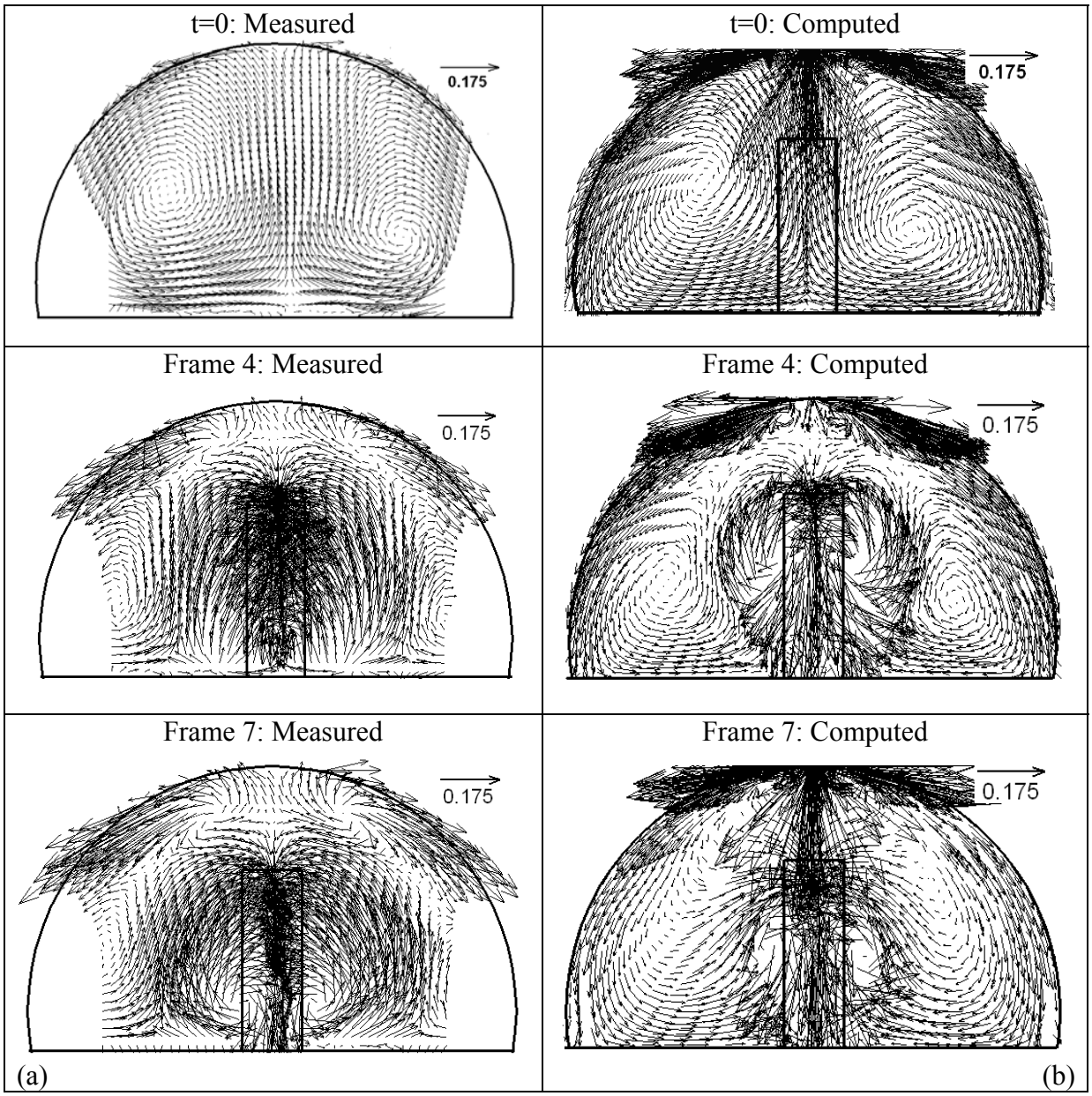

Figure 7. The (a) measured and (b) computed mean flow fields at t=0s and at Frames 4 and 7 for the case with ventilation

The interacting flow is shown in Frames 4 and 7 in Fig. 7. The strong downwash flow behind the moving body is still visible, but the lateral spread of the moving body wake is limited due to the opposing flow from the ECS. The evolution of the downwash is profoundly perturbed by the ventilation. As the body traversed through the measurement plane, the location of the vortex cores in each side of the cabin moved downward in direction of the side walls. The CFD model was able to capture this transient vortex development. However, discrepancies between the results of the CFD model and the experiments are evident. This stems from the sensitivity of the overall flow to the computed wake behind the moving body.

2. Longitudinal Flow

2.1. Baseline case

A thorough analysis of the perturbed flow in the wake of the body moving along the cabin length was conducted for the baseline and ventilation cases. Instantaneous PLIF and PIV measurements are shown in Figs. 8(a) and (b) respectively. The measurements were complemented by computed CFD data of flow (Fig. 8(c)) and contaminant transport (Fig. 8(d)). Flow structures approximately inclined at 45^o from the vertical are observed behind the moving body, as is shown in the oval marked in Fig. 8(a). Flow recirculation due to flow separation could be observed in both PIV (Fig. 8(b)) and CFD computations (Fig. 8(c)). CFD also captures the flow structures inclined at 45^o behind the moving body as shown in the oval marked in Fig. 8(c). However the longitudinal flow computed behind the moving body is much stronger than that observed in the PIV measurements; hence the longitudinal momentum transfer is over predicted. This may due to less momentum transfer in the lateral directions, thus resulting in vertically elongated eddy rings in the cabin cross section as seen earlier. A higher longitudinal momentum can lead to an over prediction of longitudinal contaminant transport and an under prediction of lateral transmission. The capability of the unsteady RANS model to accurately distribute the momentum and its subsequent implications on contaminant transport due to movement remains to be quantified. Overall, the CFD model is effective in capturing the fundamental flow mechanisms.

2.2. Ventilation case

Figure 9 shows the measured (Figs. 9(a) and (b)) and computed (Figs. 9(c) and (d)) results of the longitudinal flow and contaminant transport with cabin ventilation. The contaminant dye is observed to convect to higher vertical locations (Figs. 9 (a)). The CFD model was able to capture the vortex structure above the moving body for this case too (Figs. 9(b) and (c)). The injection of water coming into the cabin through the overhead duct is seen in the CFD results (Fig. 9(c)). As the measurement window was focused inside the cabin, the PIV measurements in Fig. 9(b) did not show these incoming jets. Figure 9 (d) shows that the convection of the contaminant dye to higher vertical locations is also captured by CFD. The mixing in the wake is modified and a shorter longitudinal recirculation region is observed for the ventilation case versus baseline case (Figs. 8(c) and 9(c)). The flow structures inclined at 45^o behind the body for the baseline case were disrupted due to the interaction of wake behind the moving body and the flow from the cabin ventilation system.

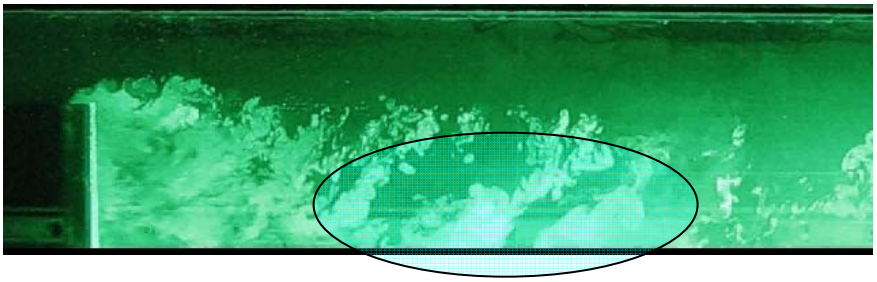

(a)

(b)

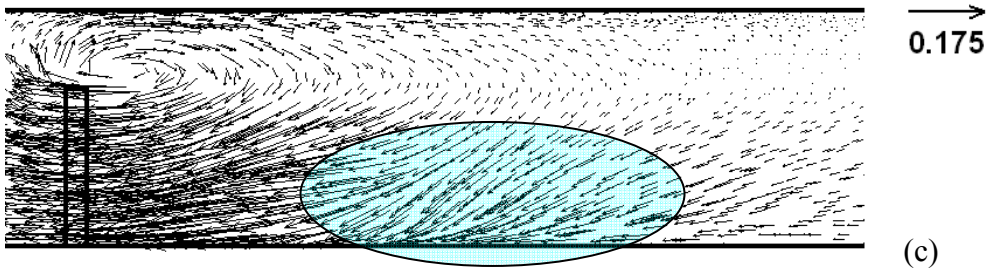

(c)

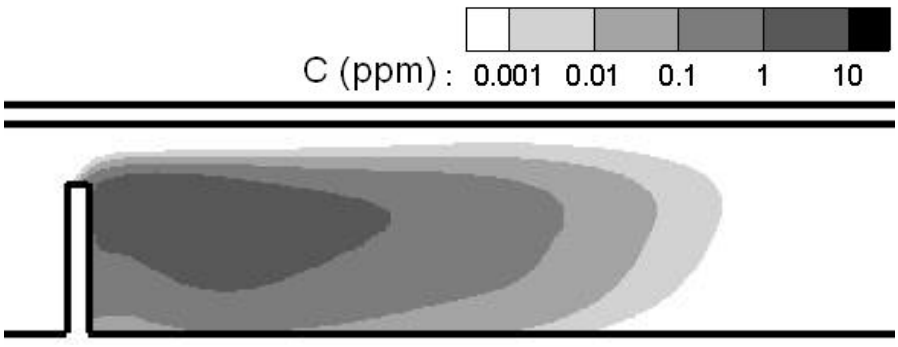

(d)

Figure 8. (a) Instantaneous flow visualization using PLIF; (b) mean measured longitudinal flow field using PIV; (c) mean computed longitudinal flow field; and (d) the computed dye concentration for the baseline case.

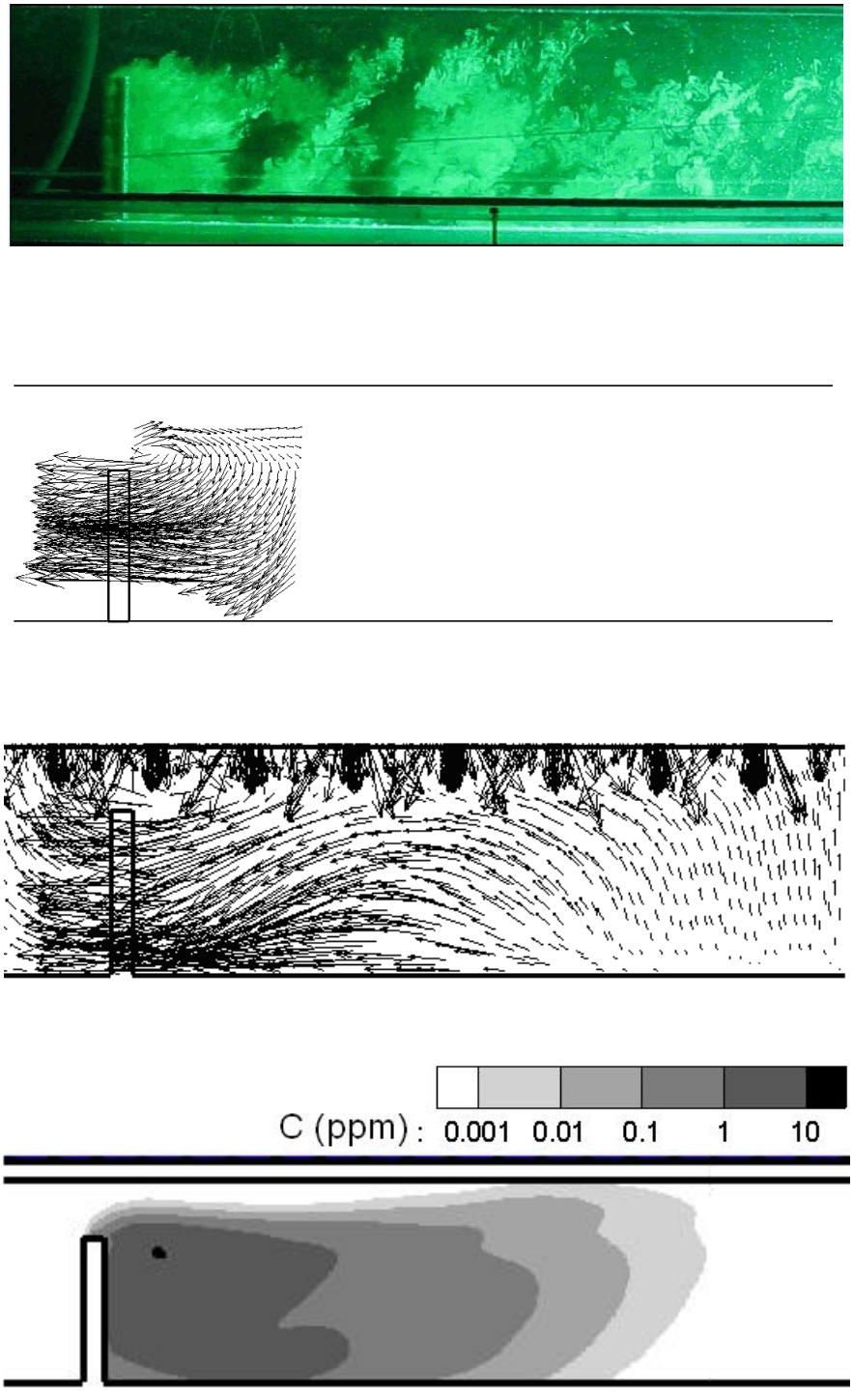

Figure 9. (a) Instantaneous flow visualization using PLIF; (b) mean velocity field using PIV; (c) mean computed longitudinal flow field; and (d) the computed dye concentration for the case with ventilation.

3. Contaminant Transport

Figures 10 and 11 show a qualitative comparison of contaminant dye transport across the cabin cross section for the baseline and ventilation cases, respectively. Twenty-five instantaneous PLIF images were averaged to obtain the measured mean concentration field. A limited number of realizations were acquired because the water tank had to be cleaned after each dye injection experiment. Twenty-five measurements were typically sufficient to observe vertical symmetry in the wake, as shown in Fig. 5. The maximum contaminant concentration occurs behind the top two corners of the moving body in both cases. The CFD model predicted the dye intensity profile and location of maximum intensity reasonably well. The intensity of the fluorescent dye across the cross section was very low for the ventilation case due to mixing, thus making the comparison of the measured and computed dye intensity difficult. Overall, the maximum concentration across the cabin cross-section is lower for the ventilation case, as expected.

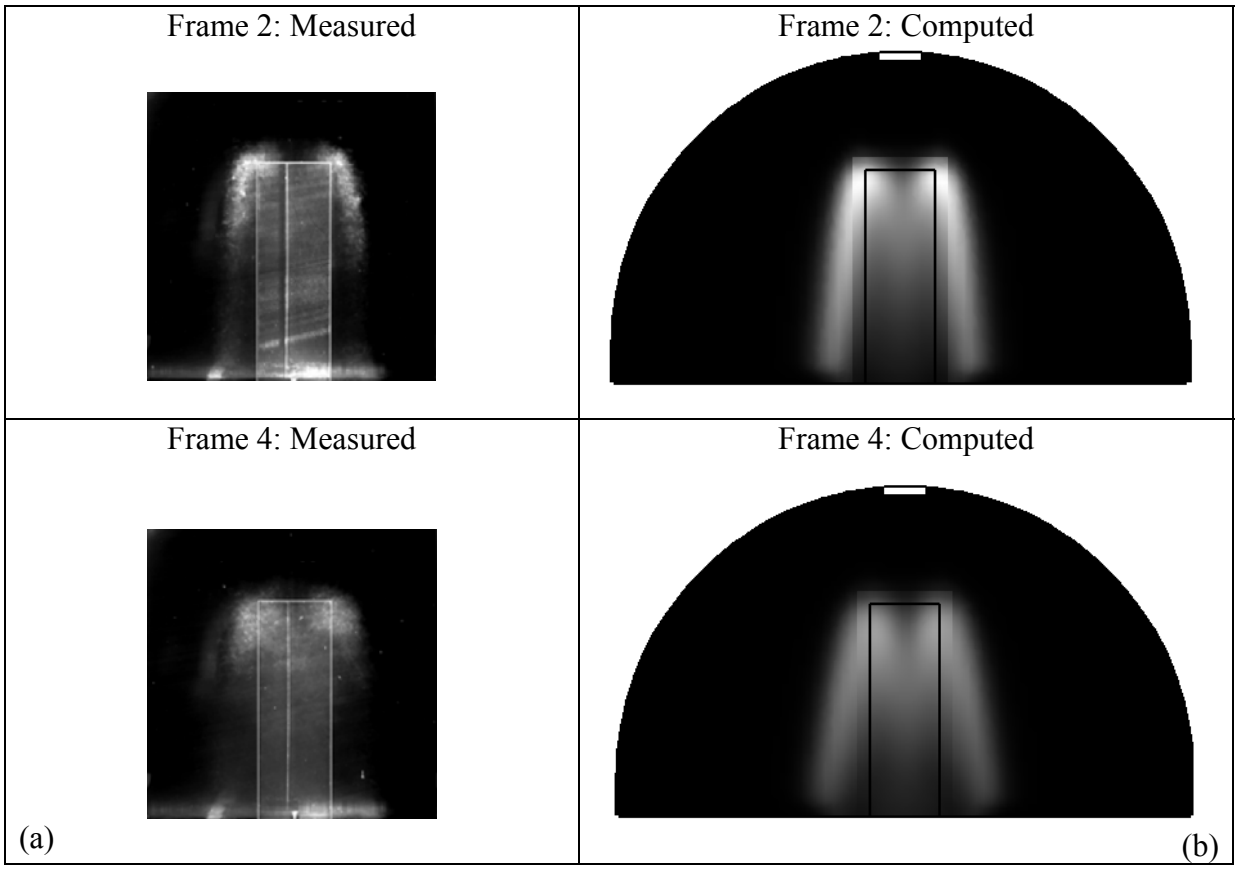

Figure 10. (a) Measured and (b) computed mean dye concentrations at Frames 2 and 4 for the baseline case.

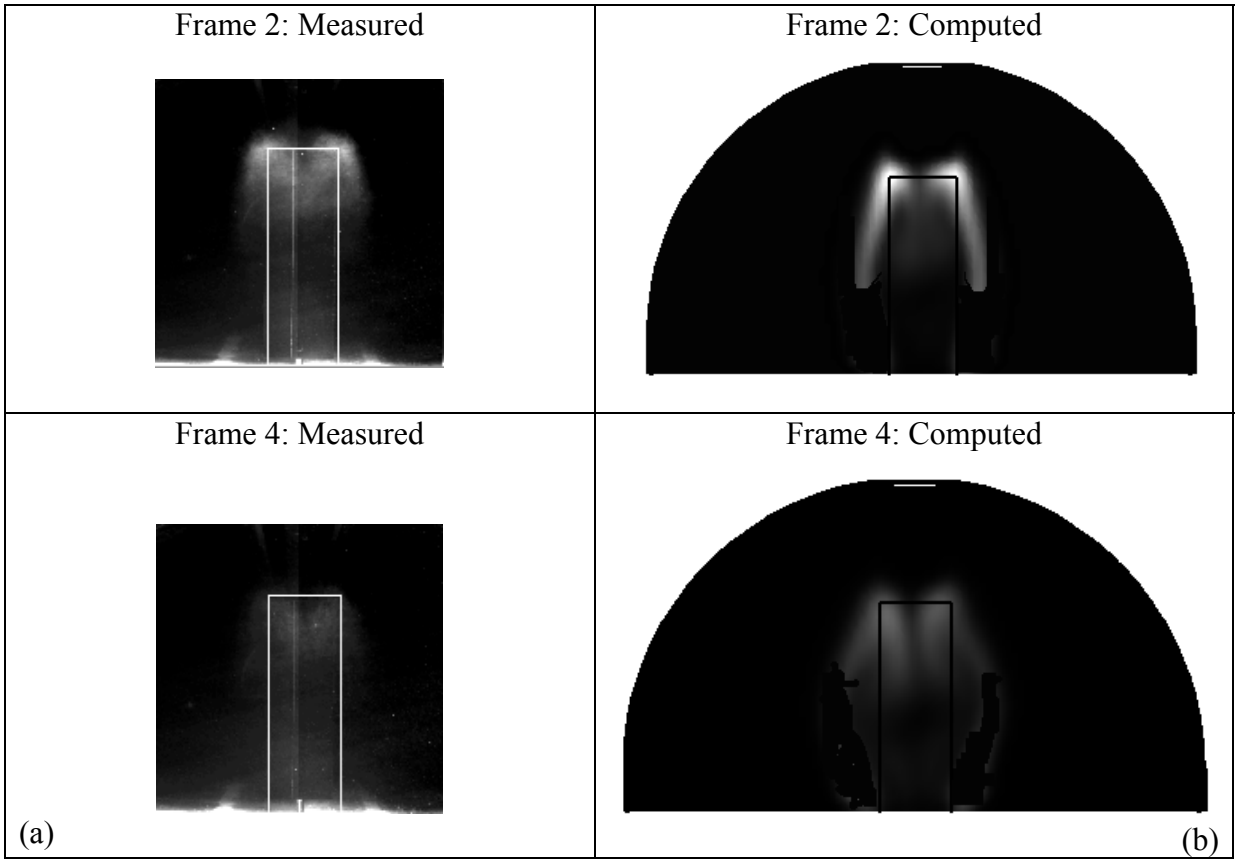

Figure 11. (a) Measured and (b) computed mean dye concentrations at Frames 2 and 4 for the ventilation case.

A quantitative comparison of the decay of contaminant concentrations across the cabin cross-section as the body moves through it is shown in Fig. 12. The decay of light intensity in the region behind the top edges of the moving body in the experiments were compared to numerical data, as this region typically showed maximum levels when compared to the rest of the flow field due to maximum dye concentration. Image processing was done using computational software (MATLAB). At Frame 4, the CFD model predicted that ventilation decreased the maximum concentration by 23% relative to the baseline case, compared with 20% reduction observed during the experiments. The magnitudes were different as the decay in light intensity/dye concentration is compared rather than the absolute concentrations. CFD predictions were within ±5% of the experimental measurements for the other frames as well. Therefore, CFD captured the comparative strength of dye concentration between the two cases remarkably well, despite the complex transient flow phenomena. Moreover, CFD

predicted that maximum dye concentration across the cabin cross section would decay by more than 30% for both cases in less than a second, i.e. from Frame 4 to Frame 10, as the body moved through. Further quantitative comparisons could not be performed due to limitations associated with the experimental technique.

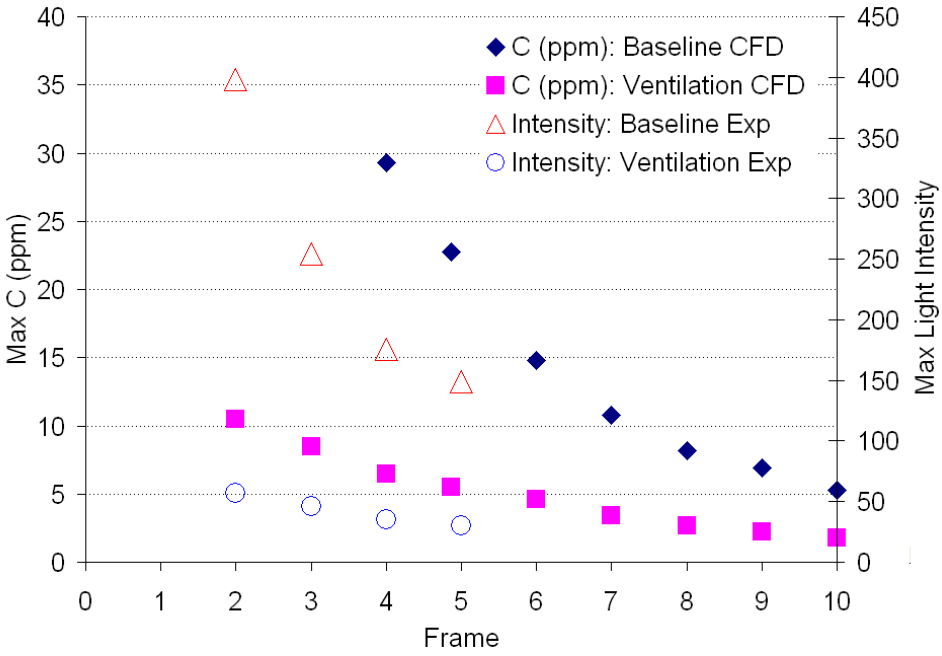

Figure 12. Comparison of the decay in maximum concentration (CFD) and dye intensity (PLIF) for the baseline and the ventilation case

CONCLUSIONS

A small-scale, water-filled model was used to investigate the effect of a moving body on flow and contaminant transport inside an airliner cabin. The small-scale model generated high quality experimental data with good spatial and temporal resolutions necessary for CFD model validation. CFD validation was done for two different conditions: one with (ventilation case) and the other without (baseline case) the cabin ECS. PIV was used to measure the flow under these two conditions. The measurements revealed a strong downwash flow along the vertical centerline of the moving body for the baseline case. The evolution of a downwash was profoundly perturbed by the flow from ECS in the ventilation case. A shorter longitudinal recirculation region was also observed for the ventilation case when compared to baseline case. The CFD model captured these fundamental flow features reasonably well. However, the CFD model predicted a higher longitudinal flow behind the moving body than that observed in the PIV measurements.

Contaminant transport predicted by the CFD model was further validated using PLIF measurements. The contaminant dye was observed to convect to higher vertical locations for

the ventilation case. The maximum contaminant concentration was found behind the top two corners of the moving body for both the cases. CFD can accurately capture this phenomenon. The CFD model was able to quantitatively estimate the change in the strength of dye concentration observed across the cabin cross section in the two cases.

ACKNOWLEDGEMENTS

This project was funded by the U.S. Federal Aviation Administration (FAA) Office of Aerospace Medicine through the National Air Transportation Center of Excellence for Research in the Intermodal Transport Environment under Cooperative Agreement 07-C-RITE-PU. Although the FAA has sponsored this project, it neither endorses nor rejects the findings of this research. The presentation of this information is in the interest of invoking technical community comment on the results and conclusions of the research.

REFERENCES

Bjørn, E., Mattsson, M., Sandberg, M. and Nielsen, P.V. 1997. Displacement Ventilation - Effects of Movement and Exhalation. *Proceedings of Healthy Buildings, 5th International Conference on Healthy Buildings*, Washington DC, USA, 2: 163 – 168.

Bjørn, E., and Nielsen, P.V. 2002. Dispersal of exhaled air and personal exposure in displacement ventilated rooms. *Indoor Air* 12: 147–164.

Brohus, H., Balling, K.D., and Jeppesen, D. 2006. Influence of movements on contaminant transport in an operating room. *Indoor Air* 16: 356-372.

Chen, Q., and Srebric, J. 2002. A procedure for verification, validation and reporting of indoor environment CFD analyses. *HVAC&R Research* 8(2): 201-216.

Choi, J.I., and Edwards, J.R. 2008. Large eddy simulation and zonal modeling of human induced contaminant transport. *Indoor Air* 18: 233–249.

Ferziger, J.H., and Peric, M. 2002. Computational Methods for Fluid Dynamics. *Springer-Verlag,* Berlin and Heidelberg, New York.

Finlayson, E.U., Gadgil, A.J., Thatcher, T.L., and Sextro, R.G. 2004. Pollutant dispersion in a large indoor space, Part 2: Computational fluid dynamics predictions and comparison with a scale model experiment for isothermal flow. *Indoor Air* 14: 272-283.

Fluent 6.2. 2003. User's Guide. FLUENT Inc.

Freymuth, P. 1993. Flow visualization in fluid mechanics. *Rev Sci Instrum*. 64:1–18.

Gendreau, M.A., and DeJohn, C. 2002. Responding to medical events during commercial airline flights. *New England Journal of Medicine* 346(14): 1067-73.

http://www.cdc.gov/mmwr/. Update: Multistate Outbreak of Mumps - United States, January 1-May 2, 2006, May 18, 2006.

Jeffrey, W.M., Cynthia, H., Michael, T.O., and Kristine, L.M. 1993. Exposure to Mycobacterium tuberculosis during air travel. *Lancet* 342: 112-113.

Joseph, S.M.P., Kwok, Y.Y., Albert, D.M.E.O, and Klaus, S. 2003. The Severe Acute Respiratory Syndrome. *New England Journal of Medicine* 349(25): 2431-41.

Kenyon, T.A., Valway, S.E., Ihle, W.W., Onorato, I.M., and Castro, K.G. 1996. Transmission of multidrug resistant mycobacterium tuberculosis during a long airplane flight. *New England Journal of Medicine* 334: 933-38.

Kühn, M., Bosbach, J., and Wagner, C. 2009. Experimental parametric study of forced and mixed convection in a passenger aircraft cabin mock-up. *Building and Environment* 44(5): 961-970.

Lakshmanan, I.A.R. 2003. Air China Flight 112: Tracking the genesis of a plague. *Boston Globe* 1A: 1.

Lin, C.H., Horstman, R.H., Ahlers, M.F., Sedgwick, L.M., Dunn, K.H., Topmiller, J.L., Bennett, J.S., and Wirogo, S. 2005. Numerical simulation of airflow and airborne pathogen transport in aircraft cabins, Part I: Numerical simulation of the flow field. *ASHRAE Transactions* 111(1): 755–763.

Lin, Y.J.P., and Linden, P.F. 2002. Buoyancy-driven ventilation between two chambers. *J.Fluid Mech.* 463: 293–312.

Lubcke, H., Schmidt, S., Rung, T., and Thiele, F. 2001. Comparison of LES and RANS in bluff-body flows. *J Wind Eng Ind Aerod* 89:1471–1485.

Matsumoto, H., Hai, N.L., and Ohba, Y. 2004. CFD simulation of air distribution in displacement ventilated room with a moving object. In: *Proceedings of Roomvent, 9th International conference on air distribution in rooms*, Coimbra, Portugal, 5-8 September.

Matsumoto, H., and Ohba, Y. 2004. The influence of a moving object on air distribution in displacement ventilated rooms. *Journal of Asian Architecture and Building Engineering* 75: 71-75.

Mattsson, M., and Sandberg, M. 1996. Velocity field created by moving objects in rooms. *Proceedings of 5th International Conference on Air Distribution in Rooms, Roomvent* Yokohama, Japan, 2: 547–554.

Mazumdar, S., and Chen, Q. 2008. Influence of cabin conditions on placement and response of contaminant detection sensors in a commercial aircraft. *Journal of Environmental Monitoring* 10: 71-81.

Musher, D.M. 2003. How contagious are common respiratory tract infections? *New England Journal of Medicine* 348: 1256-66.

NRC (National Research Council). 2002. The airliner cabin environment and the health of passengers and crew. Washington, DC: *National Academy Press*.

Olsen, S.J., Chang, H.L., Cheung, T.Y., Tang, A.F., Fisk, T.L., Ooi, S.P., Kuo, H.W., Jiang, D.D., Chen, K.T., Lando, J., Hsu, K.H., Chen, T.J., and Dowell, S.F. 2003. Transmission of the severe acute respiratory syndrome on aircraft. *New England Journal of Medicine* 349(25): 2416-22.

Poussou, S.B. 2008. Experimental investigation of airborne contaminant transport by a human wake moving in a ventilated aircraft cabin. *Ph.D. Thesis*, Purdue University.

Raffel, M., Willert, C.E., Wereley, S.T., and Kompenhans, J. 2007. Particle image velocimetry, a practical guide. *Springer-Verlag,* Berlin and Heidelberg, New York.

Samimy, M., and S. K. Lele. 1991. Motion of particles with inertia in a compressible free shear layer. *Phys Fluids* A3(8):1915–1923.

Settles, G.S. 2006. Fluid Mechanics and Homeland Security. *Annu. Rev. Fluid Mech.* 38:87–110.

Shih, Y.C., Chiu, C.C., and Wang, O. 2007. Dynamic airflow simulation within an isolation room. *Building and Environment* 42(9): 3194-3209.

Tezduyar, T.E. 2004. Finite element methods for fluid dynamics with moving boundaries and interfaces. In: Stein, E., de Borst, R., Hughes, T.J.R. (eds) *Encyclopedia of Computational Mechanics* Vol. 3: Fluids, West Sussex, England, John Wiley, 545–577, ISBN 0-470-84699-2.

Thatcher, T.L.,Wilson, D.J.,Wood, E.E., Craig, M.J., and Sextro, R.G. 2004. Pollutant dispersion in a large indoor space: Part 1—Scaled experiments using a water-filled model with occupants and furniture. *Indoor Air* 14(4):258-71.

Zhai, Z., Chen, Q., and Scanlon, P.W. 2002. Design of ventilation system for an indoor auto racing complex. *ASHRAE Transactions* 108(1), 989-998.

Zhang, Y., Sun, Y., Wang, A., Topmiller, J., and Bennett, J. 2005. Experimental characterization of airflows in aircraft cabins, Part 2: Results and research recommendations. *ASHRAE Transactions* 111(2): 53-59.

Zhang, Z., Zhang, W., Zhai, Z., and Chen, Q. 2007. Evaluation of various turbulence models in predicting airflow and turbulence in enclosed environments by CFD: Part-2: comparison with experimental data from literature. *HVAC&R Research* 13(6)*:* 871-886.

Zhang, Z., Chen, X., Mazumdar, S., Zhang, T., and Chen, Q. 2009. Experimental and numerical investigation of airflow and contaminant transport in an airliner cabin mock-up. *Building and Environment* 44(1): 85-94.